The influence of particle surface roughness on elastic stiffness and dynamic response

The influence of particle surface roughness on elastic stiffness and dynamic response

Masahide Otsubo[1], Catherine O'Sullivan[1], Kevin J. Hanley[2], Sim Way Way[3]

Affiliation
1 Department of Civil and Environmental Engineering, Imperial College London, London SW7 2AZ, UK
2 Institute for Infrastructure and Environment, School of Engineering, The University of Edinburgh, Edinburgh EH9 3JL, UK
3 Atkins, The Hub, 500 Park Avenue, Aztec West, Almondsbury, Bristol, BS32 4RZ

Keywords:
discrete element modelling; dynamics; elasticity; stiffness; waves.

ABSTRACT

Discrete element method (DEM) simulations of planar wave propagation are used to examine the effect of particle surface roughness on the stiffness and dynamic response of granular materials. A new contact model that considers particle surface roughness is implemented in the DEM simulations. Face-centred cubic lattice packings and random configurations are used; uniform spheres are considered in both cases to isolate fabric and contact model effects from inertia effects. For the range of values considered here surface roughness caused a significant reduction in stiffness, particularly at lower confining stresses. The simulations confirm that surface roughness effects can at least partially explain the value of the exponent in the relationship between stiffness and mean confining stress for an assembly of spherical particles. Frequency domain analyses showed that the maximum frequency transmitted through the sample is reduced when surface roughness is considered. The assumption of homogeneity of stress and contacts in analytical micromechanical models is shown to lead to an overestimation of stiffness.

INTRODUCTION

The elastic (small-strain) shear stiffness (G_0) of a granular material can be expressed as $G_0 \propto \sigma'^n$, where σ' = effective confining stress, and n is a constant. Hertzian contact theory combined with theoretical micromechanics gives n = 1/3 (e.g. Chang et al., 1991); however, experimental data for sands give n > 1/3. Goddard (1990) and McDowell & Bolton (2001) acknowledged that the discrepancy between Hertzian theory and experimental observations of the stress-stiffness relationship may be partially due to the presence of conical asperities (surface roughness) of real sand particles.

Experimental studies using wave propagation have consistently shown that assemblies of rougher spheres have a lower shear wave velocity (V_S) and smaller G_0 than smooth sphere assemblies (Santamarina & Cascante, 1998; Sharifipour & Dano, 2006; Otsubo et al., 2015). However, it is difficult to systematically control roughness in experiments to develop an empirical relationship between roughness and the exponent n. The analytical work of Yimsiri & Soga (2000) clearly indicated that n > 0.5 for rough materials; however the model used includes a number of simplifying assumptions. Once an appropriate contact model is available, discrete element method (DEM) simulations provide an alternative means to explore this relationship, as demonstrated in a limited analysis of a single lattice assembly by O'Donovan et al. (2015). This contribution extends the work of both O'Donovan et al. (2015) and Cavarretta et al. (2010) by proposing a new rough-surface contact model and implementing it in DEM. This model is used in simulations of stress wave propagation tests on both lattice and random samples to establish the influence of surface roughness on the G_0 - σ' relationship.

ROUGH SURFACE CONTACT MODEL

Hertzian contact mechanics gives the force-displacement relationship for the contact between two smooth spheres as (Johnson, 1985):

$$N = \frac{4}{3} E_p^* R^{*0.5} \delta^{1.5} \qquad (1)$$

where N = normal contact force, $E_p^* = [(1\text{-}\nu_{p1}^2)/E_{p1} + (1\text{-}\nu_{p2}^2)/E_{p2}]^{-1}$, $R^* = (1/R_1 + 1/R_2)^{-1}$, and δ = contact overlap. The subscripts refer to the two contacting particles; R_i = radius of particle i, E_{pi} = Young's modulus of particle i, and ν_{pi} = Poisson's ratio of particle i. Differentiating N with respect to δ gives the normal contact stiffness (k_N):

$$k_N = \left(6E_p^{*2}R^*\right)^{1/3} N^{1/3} \tag{2}$$

Asperities on real particle surfaces give a finite roughness; this can be quantified using the root mean square of surface roughness (S_q) (e.g. Thomas, 1982). Based on a theoretical study of rough contacts, Greenwood & Tripp (1967) noted that asperity deformation dominates the $N - \delta$ relationship when $N < N_{T1}$; it is only when $N \geqq N_{T2}$ that Hertzian contact mechanics becomes applicable, where

$$N_{T1} = S_q^* E^* \sqrt{2R^* S_q^*} \tag{3}$$

$$N_{T2} = 100N_{T1} = 100\ S_q^* E^* \sqrt{2R^* S_q^*} \tag{4}$$

and $S_q^* = (S_{q1}^2 + S_{q2}^2)^{0.5}$.

Cavarretta et al. (2010 & 2012) used particle compression tests to confirm the applicability of Hertzian theory when N exceeds N_{T2} and proposed the Cavarretta contact model for rough surfaces.

Referring to Fig. 1, the $N - \delta$ relationship for rough surfaces proposed here considers three stages: asperity-dominated (Eq. 5), transitional (Eq. 6), and Hertzian (Eq. 7):

$$N = N_{T1}\left(\frac{\delta}{\delta_{T1}}\right)^c \qquad N < N_{T1}\ (\delta < \delta_{T1}) \tag{5}$$

$$N = N_{T2}\left(\frac{\delta - \delta_1}{\delta_{T2} - \delta_1}\right)^b \qquad N_{T1} <= N < N_{T2}\ (\delta_{T1} <= \delta < \delta_{T2}) \tag{6}$$

$$N = \frac{4}{3}E_p^* R^{*0.5}\left(\delta - \delta_1 - \delta_2\right)^{1.5} \qquad N_{T2} <= N\ (\delta_{T2} <= \delta) \tag{7}$$

where δ_{T1} & δ_{T2} = threshold contact displacements at $N = N_{T1}$ & N_{T2}, and b & c are constants. The dimensional constants δ_1 and δ_2 control the $N - \delta$ relationship. The Cavarretta model relates δ_2 to the surface hardness (H) as:

$$\delta_2^{Cavarretta} = r\left(\frac{3\pi}{4}\frac{H}{E_p^*}\right)^2 \tag{8}$$

where r is a function of the particle radius, roundness and shape. The surface hardness may be influenced by surface roughness, making it difficult to isolate the influence of surface roughness. In the new model the threshold displacements are given by:

$$\delta_{T2} = \left(\frac{3}{4}\frac{N_{T2}}{E^* R^{*0.5}}\right)^{2/3} + \delta_1 + \delta_2 \tag{9}$$

$$\delta_{T1} = \left(\frac{N_{T1}}{N_{T2}}\right)^{1/b}\left(\delta_{T2} - \delta_1\right) + \delta_1 \tag{10}$$

The constants b and c in Eqs. 5 to 7 can be obtained by imposing a constraint that the three curves of the $N - \delta$ relationship (Eqs. 5 to 7) connect smoothly, i.e. values of $dN/d\delta$ are equal at the two boundaries, giving

$$b = 1.5\left(1 + \frac{\delta_2}{\delta_{T2} - \delta_1 - \delta_2}\right) \tag{11}$$

$$c = 100b\,\delta_{T1}\frac{\left(\delta_{T1} - \delta_1\right)^{b-1}}{\left(\delta_{T2} - \delta_1\right)^b} \tag{12}$$

This $N - \delta$ relationship still depends on δ_1 and δ_2, and they are related to S_q. Greenwood et al. (1984) introduced a roughness index (α):

$$\alpha = \frac{S_q^*}{\delta_{smooth}} \tag{13}$$

where the overlap for a smooth contact (δ_{smooth}) at a given N is obtained using Eq. 1. The smooth and rough contact radii can be calculated as $a_{smooth} = (R^* \delta_{smooth})^{0.5}$ and $a_{rough} = (R^* \delta_{rough})^{0.5}$, respectively, at a given N (Eqs. 5 to 7). Yimsiri & Soga (2000) related α to the ratio of the radius of a smooth contact to a rough contact:

$$\frac{a_{rough}}{a_{smooth}} = \left(\frac{-2.8}{\alpha + 2} + 2.4 \right) \tag{14}$$

Considering the ratio a_{rough}/a_{smooth}, Fig. 2 compares the proposed contact model with the experimental data of Greenwood et al. (1984) and the Yimsiri & Soga model. Values of δ_1=0.82S_q and δ_2=1.24S_q were obtained by iterative curve fitting to Eq. 14. A good agreement is observed. Taking $\delta_2 = \delta_2^{Cavarretta}$ (Eq. 8) and $\delta_1 = 0$ (also $N_{T1} = 0$ & $\delta_{T1} = 0$) reduces the proposed model to the Cavarretta model and when $S_q = 0$, the model is identical to Hertzian theory. The model idealises the real physical system: it does not consider yielding, squashing or vibration of asperities or the change in the inter-particle friction due to the plastic compression of asperities (Hanaor et al., 2013).

The proposed $N - \delta$ is shown in Fig. 3a & 3b for S_q values that would cover a realistic range of roughness values based on optical interferometry (Otsubo et al., 2015). It is clear that k_N decreases with increasing S_q especially at lower N values. The power coefficients relating k_N and N for rough contact can be obtained by differentiating Eqs. 5 to 7 with respect to δ, giving 0.614 ($N < N_{T1}$), 0.368 ($N_{T1} <= N < N_{T2}$), and 1/3 ($N_{T2} <= N$). For a perfectly smooth contact ($S_q = 0$), the power coefficient is 1/3 as expressed in Eq. 2. The approximately bi-linear trend can be seen in Fig. 3b with the model converging to the Hertzian curve at $N = N_{T2}$; it differs from the smooth $k_N - N$ relationship proposed by Yimsiri & Soga (2000).

Yimsiri & Soga (2000) considered the tangential contact stiffness to be the same as that of smooth contact based on experimental data by O'Connor & Johnson (1963). However, recent fundamental tribology research has found that roughness reduces the tangential contact stiffness (e.g. Gonzalez-Valadez et al., 2010; Medina et al., 2013). Referring to Otsubo et al. (2015), here k_T is taken as:

$$k_T = \frac{2(1-\nu_p)}{2-\nu_p} k_N \tag{15}$$

and partial slip prior to contact sliding is not considered. This expression is adopted in the Yimsiri & Soga (2000) analytical model below.

WAVE PROPAGATION SIMULATIONS

The new contact model was implemented in a modified version of the LAMMPS molecular dynamics code (Plimpton, 1995). Referring to Fig. 4, the lateral boundaries were periodic, while wall boundaries were placed at the bottom and top of the samples. Three types of sample were considered: face-centred cubic (FCC), random dense packing (RDP) and random loose packing (RLP). In all cases, uniform spheres with a diameter (D) of 2.54 mm were used with a particle shear modulus G_p = 25 GPa, particle Poisson's ratio ν_p = 0.2, and particle density ρ_p = 2230 kg/m^3. The surface roughness values given in Fig. 3 were used (S_q = 0, 0.5 and 1.0 μm). The same material properties and contact models were also used for wall boundaries with $R = \infty$. The time step (Δt) for the wave propagation simulations (1×10^{-9} s) was smaller than the critical time step for the Verlet time integration of 7×10^{-7} s determined via eigenmode analysis using extracted global mass and stiffness matrices. It was also significantly smaller than the period associated with the nominal input signal frequency (i.e. $1/20{,}000=5\times10^{-5}$ s). A parametric study in which Δt was varied confirmed that this time step was sufficiently small for the nonlinear contact model used.

The FCC sample consisted of 3,200 particles (4×4×200 layers) and is equivalent to that considered by Mouraille et al. (2006). Both the RDP and RLP samples consisted of 35,201 particles and were initially created as clouds of non-contacting spheres with μ = 0 and 0.15 respectively. The sample lengths (L) were 141D to 144D with aspect ratios ≈10. Using uniform spheres in the random samples enabled the effects of fabric and contact model to be isolated from any particle inertia effects; local crystallisation (i.e. a coordination number of 12) was rare, observed in less than 0.5% of particles for the RDP sample at the maximum pressure of 10 MPa. A servo-controlled compression process was applied to achieve an initial isotropic confining stress, σ' = 1 kPa. For the RDP samples, once σ' reached 1 kPa, μ was increased to 0.15 prior to subsequent additional isotropic compression. For each packing, σ' = 0.1 0.2, 0.3, 0.5, 1 and 10 MPa were considered; void ratio (e) and mean coordination number ($C_{N,\,mean}$) data are tabulated in Tables 1 & 2. Following the

approach of Magnanimo et al. (2008), μ was increased to 0.2 for all the samples before applying the input motion to avoid particle sliding and ensure the elastic response of the samples. No damping was applied to the particles during wave propagation. Referring to Fig. 4c, S-waves were generated by moving the lower transmitter boundary (at z=0) in a transverse (X) direction. A single period, phase shifted sinusoidal pulse, frequency (f) of 20 kHz, and double amplitude ($2A$) of 20 nm was used where $2A/L \simeq 5.5 \times 10^{-8}$ and $2A/D \simeq 7.9 \times 10^{-6}$. The wave propagated in the Z-direction and the stress response was recorded at the opposite boundary (z=L).

SYSTEM RESPONSE TO WAVE PROPAGATION

The particle displacements in the X-direction along a straight line extending in the Z-direction from the transmitter wall are plotted in Fig. 5 and the mean slope of the maximum points gives the S-wave velocity ($V_{S,dL/dt}$). In comparison with the smooth sample at 100 kPa, the $V_{S,dL/dt}$ for the rough sample is clearly reduced for RDP samples. Fig. 6a and 6b present the stress responses at the receiver wall ($\Delta\sigma_X$) for the FCC and RDP samples, respectively, for S_q = 0 and 1.0 μm at σ' = 0.1, 0.3 and 1 MPa. The shear wave velocity based on the peak-to-peak method ($V_{S,P\text{-}P}$) clearly decreases with increasing roughness for both the FCC and the RDP samples and the difference is more marked at lower σ'. The $V_{S,P\text{-}P}$ and $V_{S,dL/dt}$ values are summarised in Tables 1 & 2 and the $V_{S,P\text{-}P}$ data are within 3% of $V_{S,dL/dt}$.

The frequency components of the inserted and received stress responses at σ' = 0.1 and 1 MPa for the RDP sample are compared using the gain factor (the ratio of the fast Fourier transforms of the received and transmitted signals) in Fig. 7. The cut-off frequency (maximum transmitted frequency) reduces with increasing roughness. However, as σ' increases, the difference becomes less marked. No other sensitivity to contact model was observed in the frequency domain response.

Noting that $G_0 = \rho_d V_S^2$ where ρ_d = bulk density of sample, the $G_0 - \sigma'$ relationship for the three sample types and for three roughness values are presented in Fig. 8 for the $V_{S,P\text{-}P}$ data along with the results of the analytical model (Yimsiri & Soga, 2000) as discussed in earlier section. For the FCC samples a good match was observed between the DEM and analytical results. The higher G_0 values predicted by the analytical model for the random packings are due to the simplifying assumption of contact homogeneity in the model's derivation; the heterogeneity of stress distribution in granular

materials is well known from photoelastic experiments (Drescher & De Josselin de Jong, 1972) and DEM simulations (Rothenburg & Bathurst, 1989). However, the trend of the analytical results was captured by the DEM simulations.

The cumulative distributions of N at σ' = 100 kPa are compared in Fig. 9 for the three packings considered along with the values of N_{T1} (Eq. 3) for S_q=0.5 and 1.0 μm. It is clear $N<N_{T1}$ for all the contacts in the FCC sample; however for both random samples $N>N_{T1}$ for a significant proportion of the contacts at S_q=0.5 μm. This explains the more gradual change in the slope for the random samples. The proportion of contacts with $N>N_{T1}$, is higher for the RLP sample than the RDP sample as the lower coordination numbers for the RLP samples results in larger N at each contact. This may explain why the influence of surface roughness is less significant for the RLP samples (Figs. 8b and 8c).

CONCLUSIONS

This contribution has assessed the influence of surface roughness on the small-strain shear modulus (G_0) and dynamic response of granular materials using DEM simulations. A new rough-surface contact model was introduced. Planar wave propagation simulations were performed using a face-centred cubic sample and dense and loose samples of uniform spheres.

The detailed particle scale data available in the DEM simulation provided a direct measurement of the shear wave velocity ($V_{S,dL/dt}$). The $V_{S,dL/dt}$ values were within 3% of those obtained by applying the conventional peak-to-peak interpretative approach.

The shear wave velocity decreased with increasing surface roughness, with consequent reductions in G_0. The reduction in G_0 due to surface roughness was substantial at a low confining stress (σ'), whereas it gradually disappeared as σ' increased. In the frequency domain, a reduction in the maximum transmitted frequency due to increasing roughness was noted at low σ'. The surface roughness increased the power coefficient (n) in the $G_0 - \sigma'$ relationship; however as σ' increased, n approached the value for smooth contacts. This finding qualitatively agrees with prior analytical modelling by Yimsiri & Soga (2000) and Otsubo et al. (2015); the quantitative differences with the analytical model can largely be attributed to the assumption of homogeneity in the analytical model.

ACKNOWLEDGEMENTS

The first author is supported by JASSO (Japan Student Services Organization) and an Imperial College Dixon Scholarship. This research builds upon ideas developed in the joint EPSRC funded projects EP/G064954/1 and EP/G064180/1.

References

Cavarretta, I., Coop, M. & O'Sullivan, C. (2010). The influence of particle characteristics on the behaviour of coarse grained soils. *Géotechnique* **60**, No. 6, 413–423.

Cavarretta, I., O'Sullivan, C., Ibraim, E., Lings, M., Hamlin, S. & Muir Wood, D. (2012). Characterization of artificial spherical particles for DEM validation studies. *Particuology* **10**, No. 2, 209–220.

Chang, C.S., Misra, A. & Sundaram, S.S. (1991). Properties of granular packings under low amplitude cyclic loading. *Soil Dynamics and Earthquake Engineering* **10**, No. 4, 201–211.

Drescher, A. & De Josselin de Jong, G. (1972). Photoelastic verification of a mechanical model for the flow of a granular material. *Journal of the Mechanics and Physics of Solids* **20**, No. 5, 337–351.

Goddard, J.D. (1990). Nonlinear elasticity and pressure-dependent wave speeds in granular media. *Proceedings of the Royal Society A: Mathematical, Physical and Engineering Sciences* **430**, No. 1878, 105–131.

Gonzalez-Valadez, M., Baltazar, A. & Dwyer-Joyce, R.S. (2010). Study of interfacial stiffness ratio of a rough surface in contact using a spring model. *Wear* **268**, No. 3-4, 373–379.

Greenwood, J.A. & Tripp, J.H. (1967). The elastic contact of rough spheres. *Journal of Applied Mechanics* **34**, No. 1, 153–159.

Greenwood, J.A, Johnson, K.L. & Matsubara, E. (1984). A surface roughness parameter in hertz contact. *Wear* **100**, 47–57.

Hanaor, D.A.H., Gan, Y. & Einav, I. (2013). Effects of surface structure deformation on static friction at fractal interfaces. *Géotechnique Letters* **3**, No. 2, 52–58.

Johnson, K.L. (1985). *Contact mechanics*, Cambridge University Press.

Magnanimo, V., La Ragione, L., Jenkins, J.T., Wand, P. & Makse, H.A. (2008). Characterizing the shear and bulk moduli of an idealized granular material. *Europhysics Letters* **81**, No. 3, 34006.

McDowell, G. & Bolton, M. (2001). Micro mechanics of elastic soil. *Soils and foundations* **41**, No. 6, 147–152.

Medina, S., Nowell, D. & Dini, D. (2013). Analytical and numerical models for tangential stiffness of rough elastic contacts. *Tribology Letters* **49**, No. 1, 103–115.

Mouraille, O., Mulder, W.A. & Luding, S. (2006). Sound wave acceleration in granular materials. *Journal of Statistical Mechanics: Theory and Experiment* **07**, No. 23, 1–15.

O'Connor, J.J. & Johnson, K.L. (1963). The role of surface asperities in transmitting tangential forces between metals. *Wear* **6**, No. 2, 118–139.

O'Donovan, J., O'Sullivan, C., Marketos, G. & Muir Wood, D. (2015). Analysis of bender element test interpretation using the discrete element method. *Granular Matter* **17**, No. 2, 197–216.

Otsubo, M., O'Sullivan, C., Sim, W.W. & Ibraim, E. (2015). Quantitative assessment of the influence of surface roughness on soil stiffness. *Géotechnique* **65**, No. 8, 694–700.

Plimpton, S. (1995). Fast parallel algorithms for short-range molecular dynamics. *Journal of Computational Physics* **117**, No. 1, 1-19.

Rothenburg, L. & Bathurst, R.J. (1989). Analytical study of induced anisotropy in idealized granular materials. *Géotechnique* **39**, No. 4, 601–614.

Santamarina, J.C. & Cascante, G. (1998). Effect of surface roughness on wave propagation parameters. *Géotechnique* **48**, No. 1, 129–136.

Sharifipour, M. & Dano, C. (2006). Effect of grains roughness on waves velocities in granular packings. In *First Euro Mediterranean in Advances on Geomaterials and Structure-Hammamet 3-5 May Tunisia*.

Thomas, T.R. (1982). *Rough surfaces*, London: Imperial College Press.

Yimsiri, S. & Soga, K. (2000). Micromechanics-based stress–strain behaviour of soils at small strains. *Géotechnique* **50**, No. 5, 559–571.

Table 1 Shear wave velocities for FCC samples calculated using particle scale and boundary data *(values in italics and parentheses give error relative to direct measurement of wave passage (dL/dt))*

Packing	S_q (μm)	σ' (MPa)	e	$C_{N,\,mean}$	$V_{S,\,dL/dt}$ (m/s)	$V_{S,\,P\text{-}P}$ (m/s)	
FCC	0	0.1	0.353	12.0	544.5	542.2	*(-0.4%)*
FCC	0	0.2	0.352	12.0	612.2	609.7	*(-0.4%)*
FCC	0	0.3	0.352	12.0	655.8	652.4	*(-0.5%)*
FCC	0	0.5	0.352	12.0	715	710.0	*(-0.7%)*
FCC	0	1	0.351	12.0	803.6	795.8	*(-1.0%)*
FCC	0	10	0.341	12.0	1174.5	1166.6	*(-0.7%)*
FCC	0.5	0.1	0.352	12.0	431.6	431.4	*(0.0%)*
FCC	0.5	0.2	0.351	12.0	534.8	532.8	*(-0.4%)*
FCC	0.5	0.3	0.351	12.0	604.2	602.0	*(-0.4%)*
FCC	0.5	0.5	0.350	12.0	664.8	661.3	*(-0.5%)*
FCC	0.5	1	0.349	12.0	756.1	750.2	*(-0.8%)*
FCC	0.5	10	0.339	12.0	1151.8	1144.4	*(-0.6%)*
FCC	1	0.1	0.351	12.0	372.6	373.3	*(0.2%)*
FCC	1	0.2	0.351	12.0	461.4	460.8	*(-0.1%)*
FCC	1	0.3	0.350	12.0	523	521.3	*(-0.3%)*
FCC	1	0.5	0.349	12.0	613.1	611.2	*(-0.3%)*
FCC	1	1	0.348	12.0	742.5	736.7	*(-0.8%)*
FCC	1	10	0.337	12.0	1130.2	1123.6	*(-0.6%)*

Table 2 Shear wave velocities for random samples calculated using particle scale and boundary data *(values in italics and parentheses give error relative to direct measurement of wave passage (dL/dt))*

Packing	S_q (μm)	σ' (MPa)	e	$C_{N,\,mean}$	$V_{S,dL/dt}$ (m/s)	$V_{S,P\text{-}P}$ (m/s)	
RDP	0	0.1	0.544	6.02	365.1	368.4	*(0.9%)*
RDP	0	0.2	0.543	6.07	411.4	414.7	*(0.8%)*
RDP	0	0.3	0.543	6.10	441.8	444.7	*(0.7%)*
RDP	0	0.5	0.542	6.15	483.1	485.9	*(0.6%)*
RDP	0	1	0.540	6.24	546.1	548.6	*(0.5%)*
RDP	0	10	0.519	6.69	831	830.9	*(0.0%)*
RDP	0.5	0.1	0.544	6.13	323.5	326.5	*(0.9%)*
RDP	0.5	0.2	0.543	6.16	381.5	384.4	*(0.8%)*
RDP	0.5	0.3	0.543	6.19	414.4	416.8	*(0.6%)*
RDP	0.5	0.5	0.542	6.23	457.3	459.7	*(0.5%)*
RDP	0.5	1	0.539	6.30	523.4	524.7	*(0.3%)*
RDP	0.5	10	0.518	6.70	826.8	825.3	*(-0.2%)*
RDP	1	0.1	0.541	6.16	281.9	283.9	*(0.7%)*
RDP	1	0.2	0.540	6.20	348.6	351.3	*(0.8%)*
RDP	1	0.3	0.539	6.22	393.2	394.6	*(0.4%)*
RDP	1	0.5	0.538	6.25	444.8	446.2	*(0.3%)*
RDP	1	1	0.536	6.31	513.5	513.6	*(0.0%)*
RDP	1	10	0.514	6.72	812.9	811.2	*(-0.2%)*
RLP	0	0.1	0.646	5.03	300.7	305.8	*(1.7%)*
RLP	0	0.2	0.645	5.12	342.9	348.8	*(1.7%)*
RLP	0	0.3	0.644	5.17	371.1	376.8	*(1.5%)*
RLP	0	0.5	0.643	5.25	409.8	415.8	*(1.5%)*
RLP	0	1	0.640	5.36	469.5	475.8	*(1.3%)*
RLP	0	10	0.613	5.91	748.6	752.3	*(0.5%)*
RLP	0.5	0.1	0.646	5.21	265.5	272.2	*(2.5%)*
RLP	0.5	0.2	0.645	5.28	315.2	322.0	*(2.2%)*
RLP	0.5	0.3	0.644	5.33	345.5	352.6	*(2.0%)*
RLP	0.5	0.5	0.642	5.40	387	394.1	*(1.8%)*
RLP	0.5	1	0.639	5.50	450.6	457.6	*(1.6%)*
RLP	0.5	10	0.611	5.98	747	751.6	*(0.6%)*
RLP	1	0.1	0.643	5.28	237.1	244.1	*(3.0%)*
RLP	1	0.2	0.641	5.34	294.4	302.0	*(2.6%)*
RLP	1	0.3	0.640	5.38	330.2	337.5	*(2.2%)*
RLP	1	0.5	0.638	5.44	375.7	382.6	*(1.8%)*
RLP	1	1	0.635	5.54	442.1	447.4	*(1.2%)*
RLP	1	10	0.607	6.01	734.7	738.9	*(0.6%)*

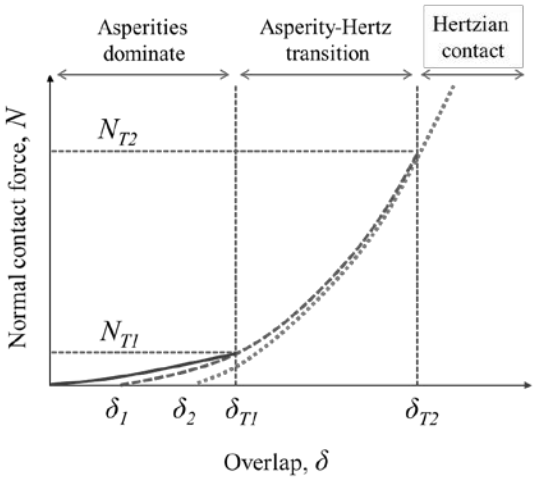

Fig. 1 Schematic illustration of proposed model for normal contact interaction.

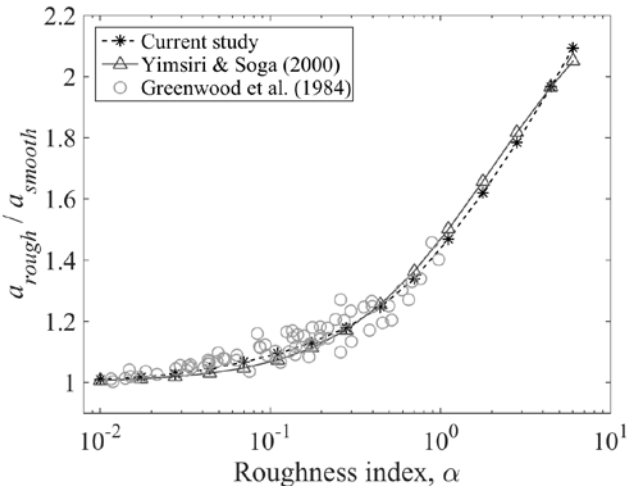

Fig. 2 Comparison of proposed model with published relationships: variation in rough / smooth contact radius ratio with roughness index.

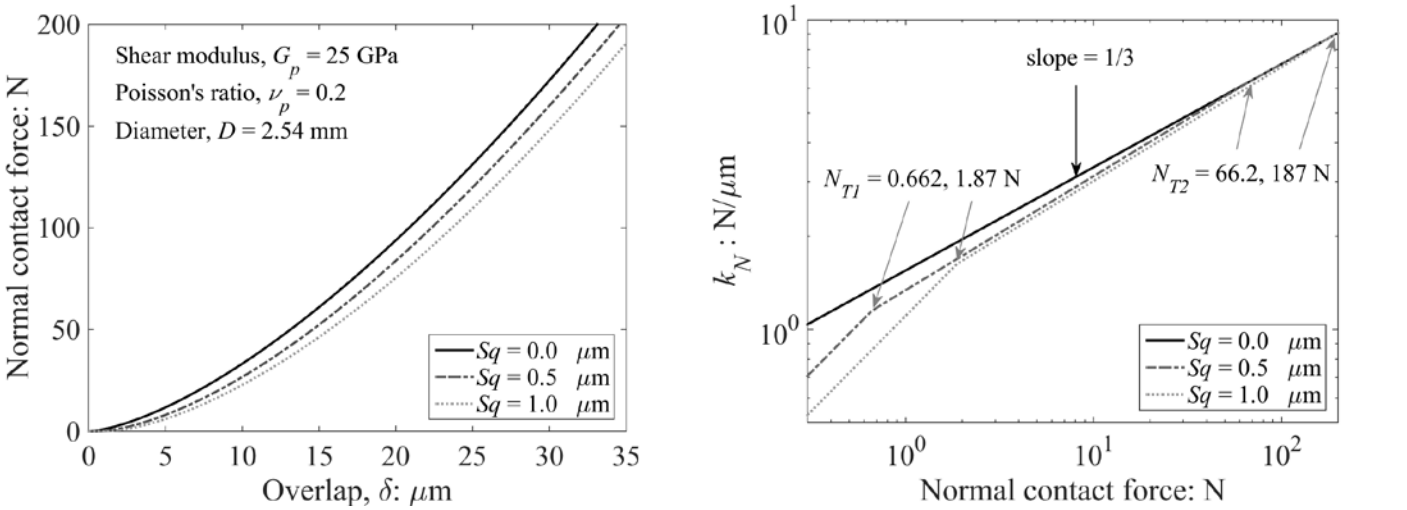

Fig. 3 Proposed model response for two particles in contact: (a) Normal contact force – Overlap, and (b) Normal contact stiffness - Normal contact force.

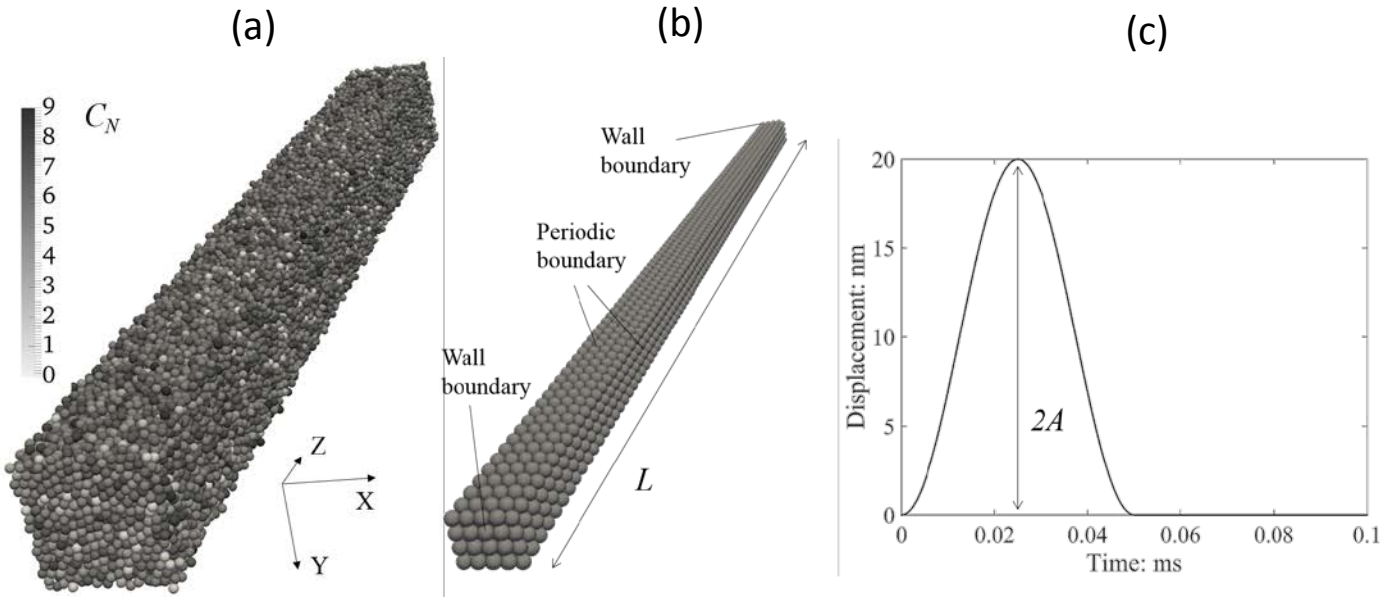

Fig. 4 (a) RLP sample and (b) FCC sample at σ' = 1 kPa with periodic boundaries in X and Y, and wall boundaries in Z. Particle shading indicates coordination number (C_N) in (a); (c) Time history of wall input motion in X direction.

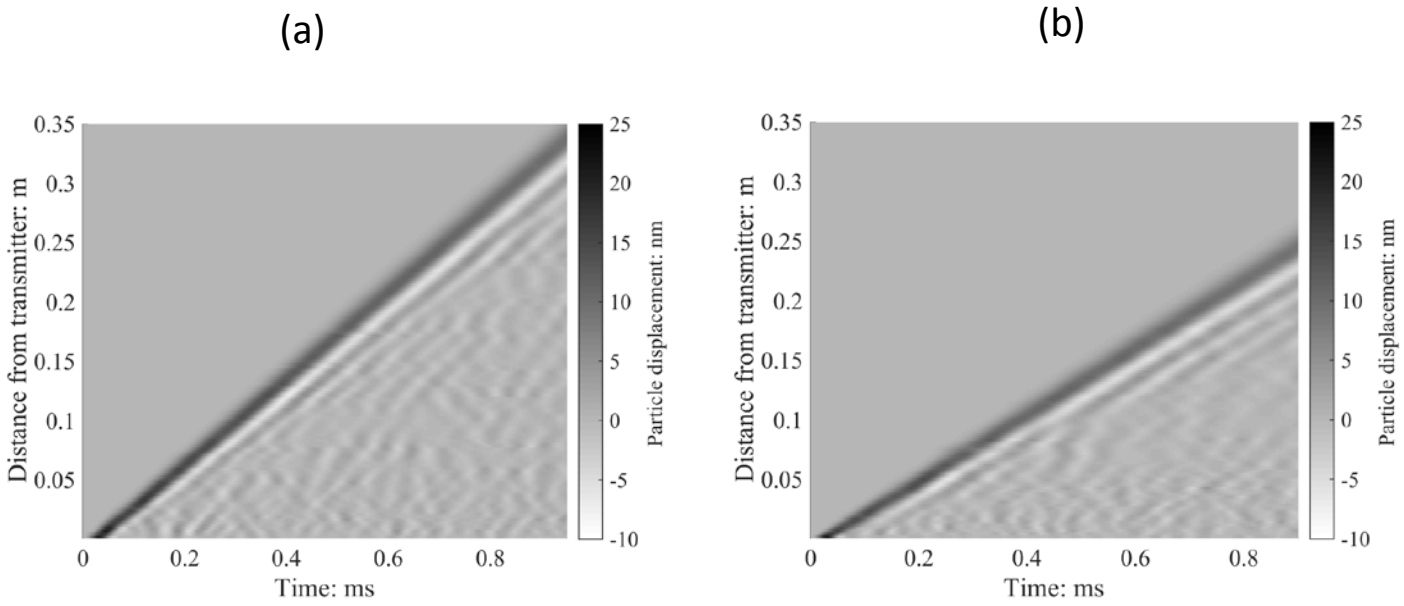

Fig. 5 Time history of particle displacements in excitation (X) direction at distances from transmitter wall (z) at σ' = 100 kPa (RDP sample) for (a) S_q = 0 μm (smooth), and (b) S_q = 1.0 μm.

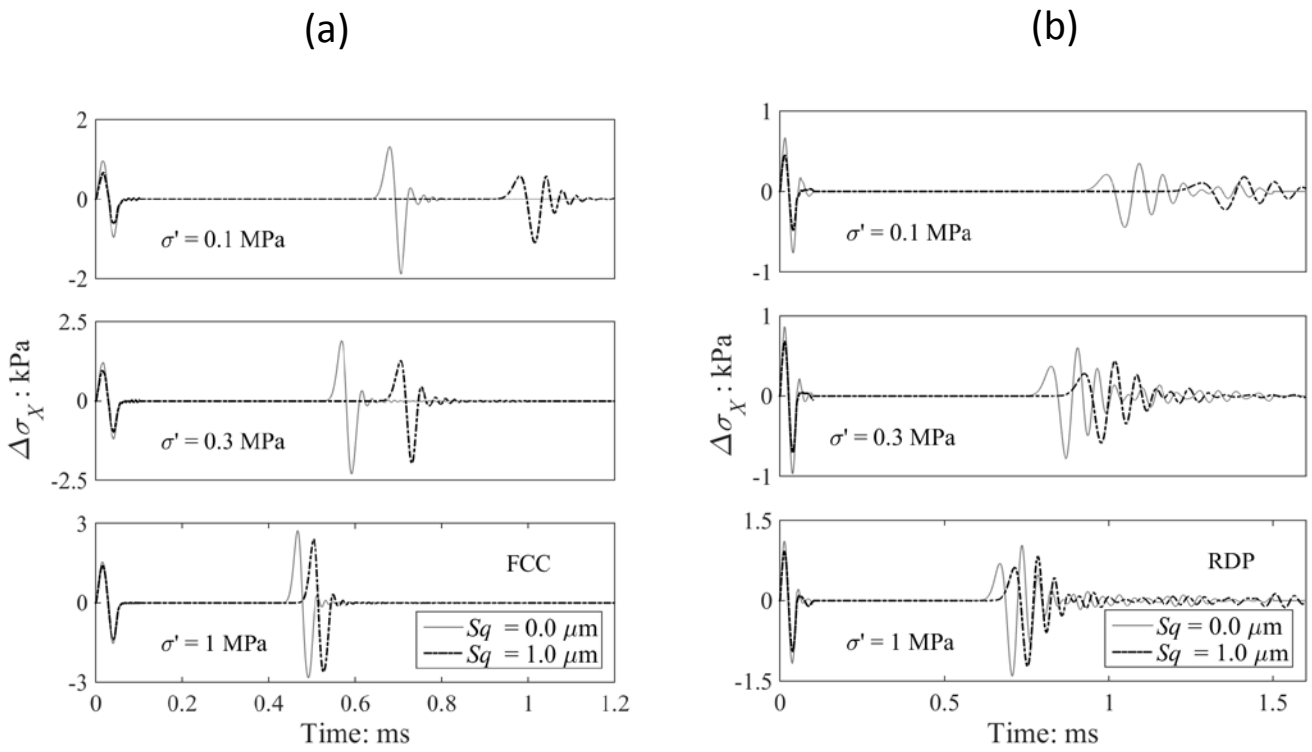

Fig. 6 Time history of increment in shear stress in excitation (X) direction on transmitter and receiver walls ($\Delta\sigma_X$) for S_q = 0.0 μm and 1.0 μm at σ' = 0.1 MPa, 0.3 MPa and 1 MPa for: (a) FCC, and (b) RDP.

(a) (b)

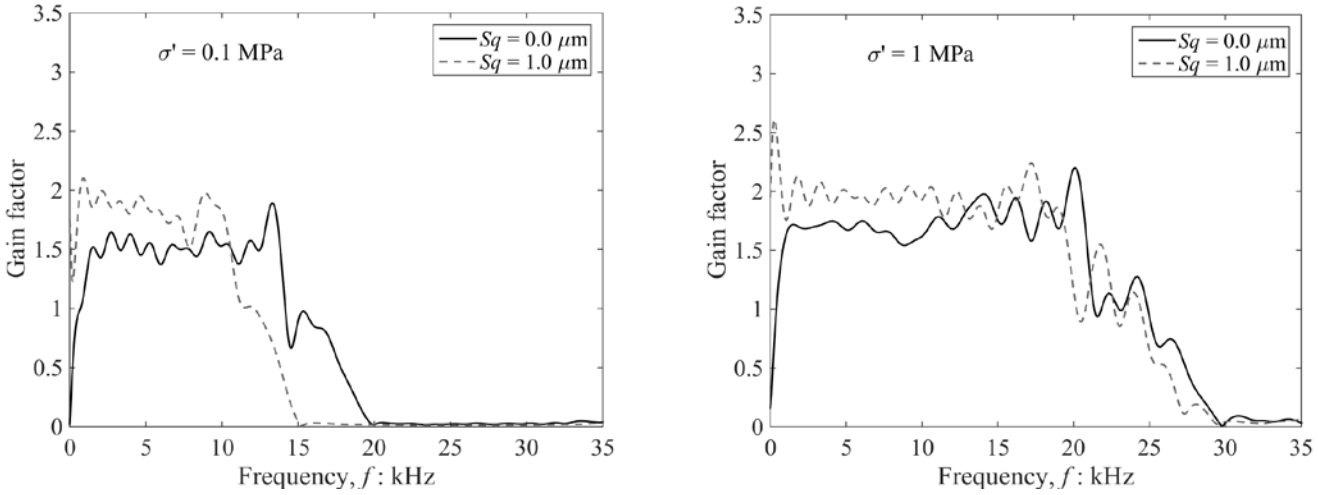

Fig. 7 Gain factor of incremental shear stress on transmitter and receiver walls for S_q=0 and S_q=1.0 μm at: (a) σ' = 0.1 MPa, and (b) σ' = 1 MPa.

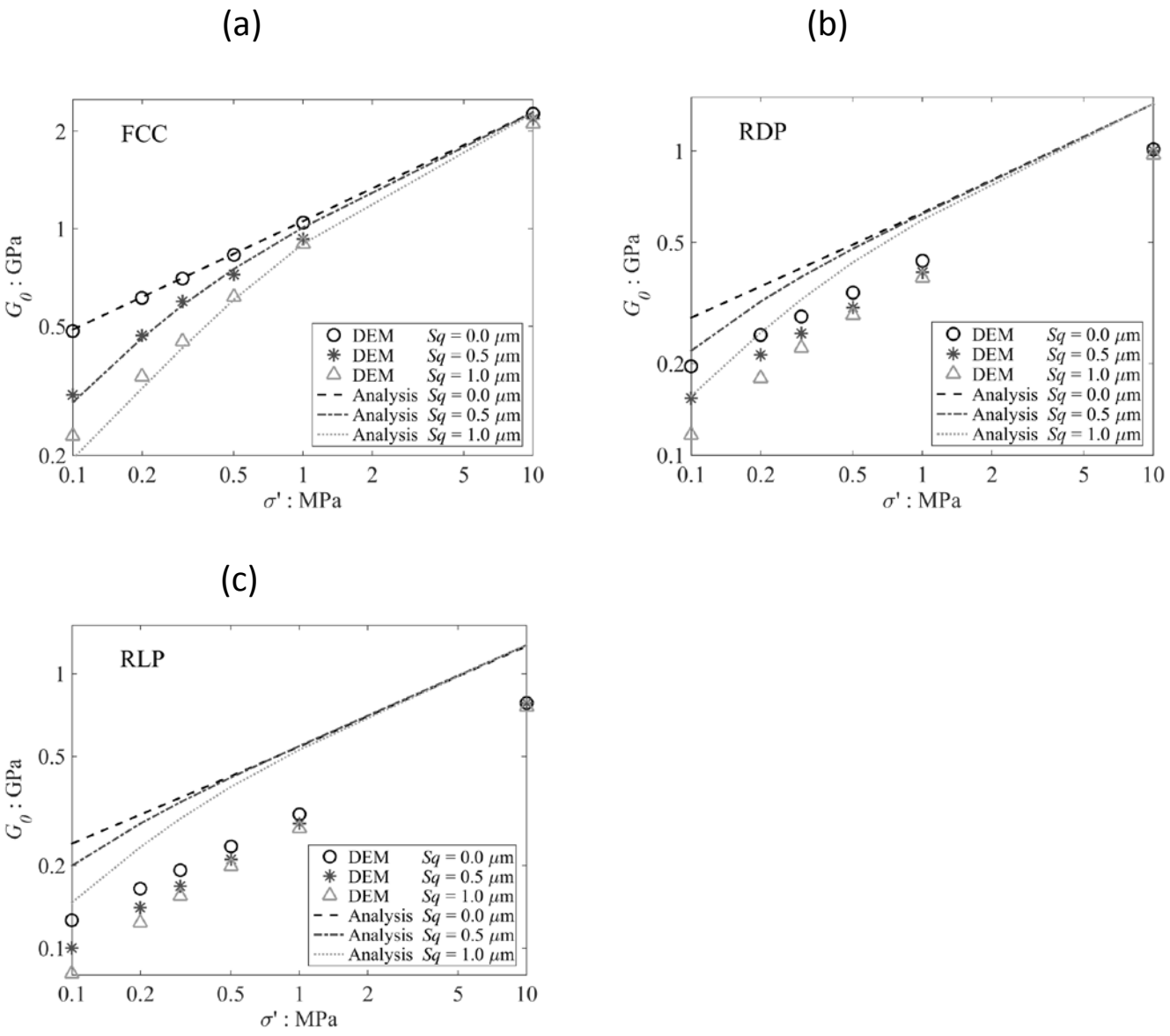

Fig. 8 Influence of surface roughness on small-strain shear modulus obtained by analytical approach and DEM results – relationship between G_0 and σ': (a) FCC, (b) RDP, and (c) RLP.

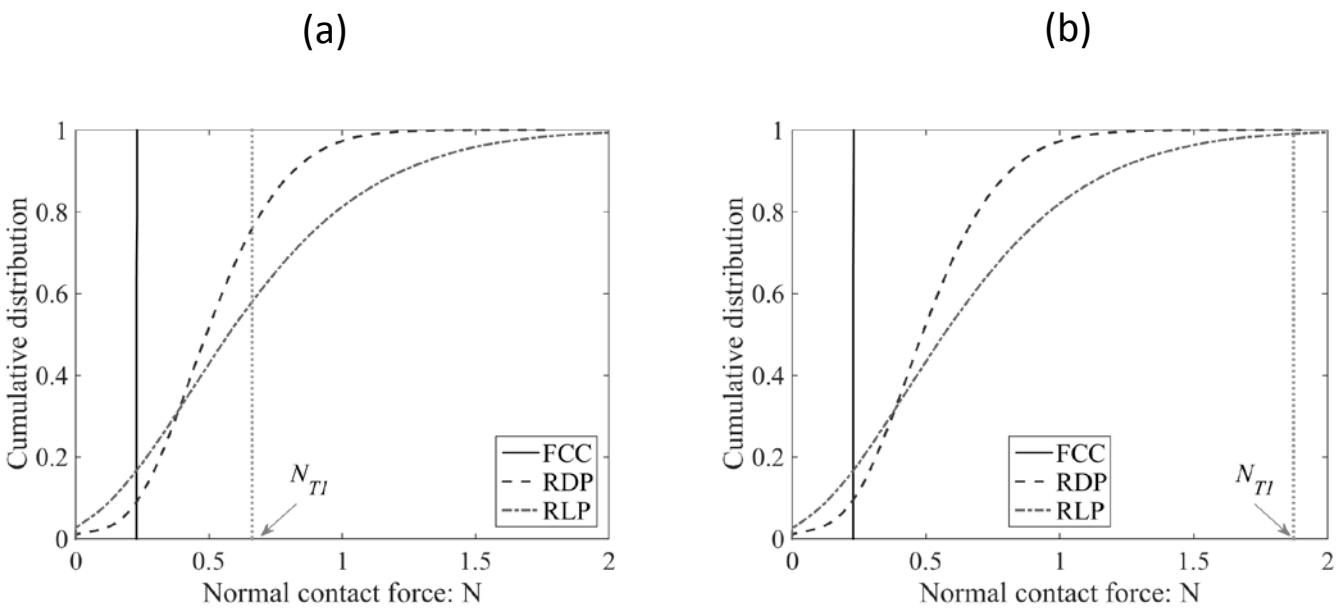

Fig. 9 Cumulative distributions of normal contact forces for different packings at p' = 100 kPa: (a) S_q = 0.5 μm, and (b) S_q = 1.0 μm.